Interplay of structural instability and lattice dynamics in Ni_2MnAl

Tarik Mehaddene, Jürgen Neuhaus, and Winfried Petry
Physik-Department E13, Technische Universität München, Forschungsneutronenquelle Heinz Maier-Leibnitz, D-85747 Garching, Germany

Klaudia Hradil
Forschungsneutronenquelle Heinz Maier-Leibnitz, D-85747 Garching, Germany and Georg-August-Universität Göttingen, Institut für Physikalische Chemie, D-37077 Göttingen, Germany

Philippe Bourges
Laboratoire Léon Brillouin (LLB), CEA Saclay, F-91191 Gif sur Yvette Cedex, France

Arno Hiess
Insitut Laue Langevin (ILL), F-38042 Grenoble Cedex 9, France
(Received 5 July 2008; published 16 September 2008)

We report on the structural instability of Ni_2MnAl from calorimetry measurements and inelastic neutron scattering. The acoustic and optical phonon dispersions along the high-symmetry $[\xi 00]$, $[\xi\xi 0]$, and $[\xi\xi\xi]$ directions have been interpolated from the normal modes of vibration using the Born–von Kármán model. The tendency of Ni_2MnAl to undergo a martensitic transformation shows up in the anomalous phonon softening of the particular $TA_2[\xi\xi 0]$ phonons in the ξ range 0.1–0.25 rlu of two different crystals. The phonon frequencies of this branch scale inversely with the valence electron concentration in good agreement with *ab initio* calculations. Contrary to the prediction of first-principles calculations in the Heusler $L2_1$-Ni_2MnAl, no anomaly is seen in the optical phonons measured in B2-Ni_2MnAl. The anomalous $TA_2[\xi\xi 0]$ phonon softening is not enhanced below room temperature when Ni_2MnAl orders in the antiferromagnetic state.

DOI: 10.1103/PhysRevB.78.104110 PACS number(s): 63.20.−e, 78.70.Nx

I. INTRODUCTION

Martensitic materials undergo a diffusionless structural phase transition in which the underlying crystal distorts from the symmetric high-temperature phase called *austenite* to the low-symmetry, low-temperature phase called *martensite*.[1] Some of them have the ability to recover large stress-induced deformations by heating the alloy through the martensitic transition temperature. They are known as shape-memory materials.[2] The tendency of shape-memory alloys to undergo a martensitic transition shows up in the dynamical properties of their underlying lattice in the austenitic phase. Usually, the frequencies of normal modes of vibration decrease with increasing temperature due to anharmonic interactions at high temperature. This temperature dependence is, however, opposite for some particular phonon modes whenever the lattice is structurally instable and shows a tendency to undergo a martensitic transition. This opposite temperature dependence, namely the decrease in the phonon frequencies with decreasing temperature, is called anomalous phonon softening. For instance, the natural instability of group-III and group-IV metals toward the formation of close-packed structures is caused by the low-restoring forces against specific atomic displacements easily identified from the phonon anomaly of the $TA_2[\xi\xi 0]$ modes.[3,4] These modes correspond to phonons propagating along the [110] direction with transverse polarization along $[1\bar{1}0]$. The $TA_2[\xi\xi 0]$ phonons have attracted the attention of many scientists and have been the subject of numerous studies not only in the pure elements but also in a number of shape-memory alloys. The dispersions of the $TA_2[\xi\xi 0]$ phonons compare well in different Cu-based alloys with a value at the zone boundary of approximately 1 THz.[5–7] The character of the anomalous phonon softening in Cu-based alloys suggests that the low-temperature phase cannot be exclusively determined by the anomaly in the $TA_2[\xi\xi 0]$ branch; rather, the final structure selected by the alloy depends on other details of the internal energy.[7] Contrary to Cu-based alloys, the phonon anomaly observed in Ni-based alloys is system specific. Its amplitude and its extension in the **q** space depend on the material and, within the same alloy system on the chemical composition.[8–10] Among Ni-based alloys, the Heusler Ni_2MnGa system is of particular interest owing to its magnetic properties. This system undergoes a martensitic transition within its ferromagnetic phase in which the shape recovery can be explored by an external magnetic field. In the martensitic state, the application of a magnetic field can cause strains up to about 10%.[11] Ni-Mn-Al and Ni-Mn-Ga are isoelectronic at equal Ga and Al concentrations when the Ni and Mn contents are kept constant. Stoichiometric Ni_2MnAl is structurally stable down to the lowest temperatures, but martensitic transformations occur in the slightly off-stoichiometric compounds, and their mechanical properties are more favorable than those of the relatively brittle Ni_2MnGa. Ni_2MnAl could be an alternative material if its magnetic shape-memory properties are as favorable as those of Ni_2MnGa. Ni_2MnAl orders in the B2 phase (CsCl) at high temperature.[12] A next-nearest-neighbor ordering develops at low temperature and the Heusler $L2_1$ phase appears.[13] However, x-ray and magnetization measurements showed that although a single B2 phase can be stabilized at room temperature by quenching from high tempera-

ture, a single $L2_1$ phase is not stabilized even after long-time annealing. A mixed state occurs which incorporates ferromagnetic ($L2_1$) the antiferromagnetic (B2) parts with close-lying Curie and Néel temperatures.[14]

Lattice dynamics measurements using inelastic neutron scattering on single crystals offer a powerful tool for investing the dynamical precursors of structural transformations on the atomic scale. Most of the phonon measurements performed on shape-memory alloys were restricted so far to the acoustic $TA_2[\xi\xi 0]$ modes. Getting more insight into the interatomic force constants and phonon-related thermodynamic properties of these alloys, however, requires the determination of the normal modes of vibration of acoustic as well as optical phonons in other high-symmetry directions. Recent first-principles calculations of the dynamical properties of Heusler alloys suggest that the phonon anomalies are not restricted to acoustic modes only.[15] Optical phonons might be as important as the anomaly in the $TA_2[\xi\xi 0]$ modes and have to be considered in order to explain the structural instability shape-memory alloys. In this paper, we report on the interplay of the lattice instability and vibrational properties of Ni_2MnAl. The temperature dependence and the effect of chemical composition on the phonon spectra are investigated. In Sec. II, measurements of the martensitic start temperature as a function of the chemical composition and heat treatment are reported. Section III contains the experimental details of the inelastic neutron scattering together with the results of the measurements in terms of the temperature and composition dependence of the normal mode of vibrations. We finally conclude on the interplay of the lattice instability and the phonon modes in Sec. IV.

II. MARTENSITIC TRANSITION IN Ni_2MnAl

The martensitic transition in different Ni_2MnAl alloys has been characterized using differential scanning calorimetry (DSC). Three sets of Ni_2MnAl alloys each with a fixed composition in Ni, Al, and Mn have been prepared using an arc-melting furnace under argon atmosphere starting from 5N7 Ni, 4N Al, and 4N Mn pure materials. The samples have been remelted several times and annealed in fused-quartz tubes under argon atmosphere during 72*h* and subsequently water quenched. The calorimetric measurements were performed by a heat-flux differential scanning calorimeter from Scientific Rheometrics. The measurements were carried out by heating up and cooling down at a constant rate of 15 K/min. An example of a DSC chart is shown in the inset of Fig. 1. The martensitic start temperature (M_s) is defined as being the crossing of the baseline with the peak tangent upon cooling down from austenite to martensite. We discuss in the following the effect of the chemical composition and heat treatment on M_s.

The impact of the individual elements on the measured M_s is depicted in Fig. 1. M_s depends strongly on composition and is connected to the individual atomic contents in a linear fashion yielding different slopes for the different elements: the rate $\Delta M_s/\Delta x$ equals −25, −35.4, and −62 K/at. % where x denotes the Mn content in $Ni_{75-x}Mn_xAl_{25}$, Al content in $Ni_{50}Mn_{50-x}Al_x$, and Al content in $Ni_{75-x}Al_xMn_{25}$, respectively. Al has the strongest influence on M_s because of its number of valence electrons which differs most strongly from the average value in stoichiometric Ni_2MnAl. If plotted against the average number of valence electrons per atom (e/a), the measured M_s values of all samples lie on a single line well fitted by a linear regression yielding $M_s[K] = 870(e/a) - 6356$ (Fig. 2). The data are compared to other Heusler Ni-based alloys from earlier works.[16–18] The data are well fitted with linear regressions yielding different slopes for different alloy systems. This behavior supports the idea that e/a does not have a universal character for the Heusler alloys. Therefore, the concentration weighted valence electron per atom e/a can be considered as an order parameter or a guideline for the occurrence of structural instabilities only

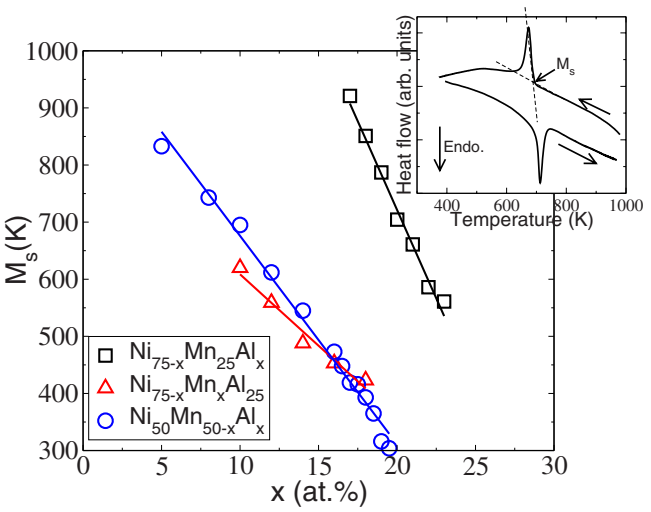

FIG. 1. (Color online) Martensitic start temperature measured on as-quenched $Ni_{75-x}Mn_{25}Al_x$, $Ni_{75-x}Mn_xAl_{25}$, and $Ni_{50}Mn_{50-x}Al_x$ samples using differential scanning calorimetry. The inset shows a typical DSC chart measured on as-quenched $Ni_{50}Mn_{40}Al_{10}$ sample upon heating up and cooling down.

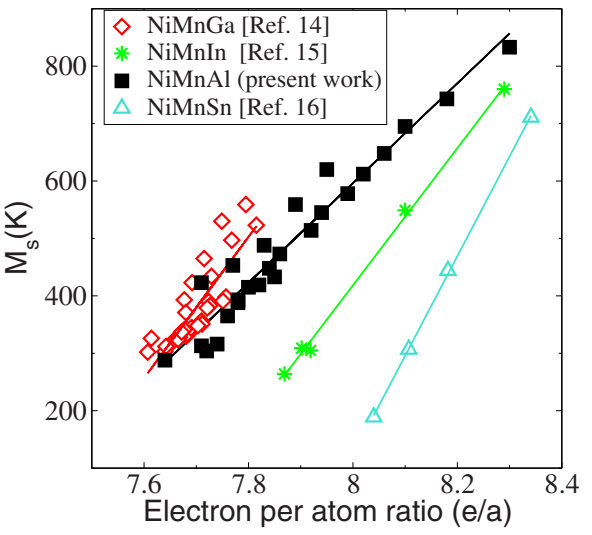

FIG. 2. (Color online) M_s versus the average number of valence electrons per atom (e/a) in different Ni-based systems. The linear regression fits to the data are shown in solid lines.

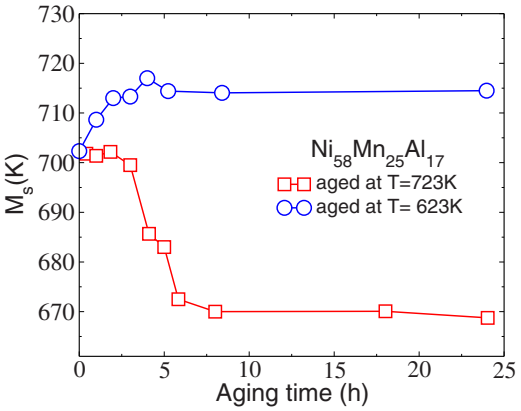

FIG. 3. (Color online) M_s versus aging time measured in different $Ni_{58}Mn_{25}Al_{17}$ samples annealed in the austenitic state at 723 K (squares) and in the martensitic state at 623 K (circles).

within a single-alloy system. For instance, a study on isoelectronic alloys obtained by substituting In for Ga to obtain Ni-Mn-Ga-In shows that, although e/a remains unchanged, the structural and magnetic transition temperatures vary considerably.[19] Based on the linear composition dependence of M_s presented above, the martensitic start temperature in Ni_2MnAl can be evaluated as $M_s[K]=2344-60.9x_{Al}-26.1x_{Mn}$, where x_{Al} and x_{Mn} are the atomic percent numbers of Al and Mn, respectively.

The effect of aging in the austenitic and martensitic states on the martensitic transformation has been investigated on a $Ni_{58}Mn_{25}Al_{17}$ sample. The M_s transformation temperature of the as-quenched $Ni_{58}Mn_{25}Al_{17}$ sample was found to be 702 K. Several pieces have been cut from the same $Ni_{58}Mn_{25}Al_{17}$ ingot. They have been aged during different times at 723 and 623 K in the austenitic and martensitic phase, respectively (Fig. 3). Generally, an extension of the existence range of the respective phase is observed. Aging in the martensitic state performed at 623 K, revealed a typical influence of aging of a shape-memory material in the martensitic state, i.e., an increase in M_s due to the thermal stabilization of martensite. Contrary to aging in the martensitic state, aging in the austenitic state results in a marked change in the martensitic transformation temperature. As evident from Fig. 3, in the early stage of aging in the austenitic phase, the change in M_s is relatively small but after $3h$ aging M_s starts to decrease strongly with aging time. At $t \geq 7h$ M_s is equal to 668 K, 34 K lower than the measured M_s in the as-quenched sample before aging. On one hand, if one considers that the samples after water quenching have a high concentration of vacancies, which is enhanced by the significant deviation of the studied composition from stoichiometry, the high density of vacancies can actually produce a permanent strain in the samples due to static atomic displacements. In this sense, the high density of vacancies is equivalent to an internal stress, leading to an increase in M_s. Aging of the samples above the martensitic transformation followed by a subsequent furnace cooling results in a drastic decrease in the density of vacancies. This process is equivalent to the release of the internal stress, decreasing the martensitic transformation temperature. On the other hand, the relatively high aging time can induce precipitation of a second phase within the B2 austenite changing by the way its e/a ratio on which the martensitic transition temperature is strongly dependent. Indeed, DSC measurements on as-prepared $Ni_{50}Mn_{50-x}Al_x$ samples (not shown here) with Al content higher than 10 at. % did not undergo any martensitic transition unless they are annealed and subsequently water quenched. This can be due to the presence of Al-rich precipitates within the B2 matrix. Indeed the B2 phase of Ni_2MnAl is stable only at high temperature.[20] It can be retained, however, by fast cooling (quenching). A slow cooling results irremediably in a phase separation.

III. NEUTRON SCATTERING

Normal modes of vibration in Ni_2MnAl have been measured by inelastic neutron scattering using the three-axis spectrometers: 2T1 near Orphée reactor at the Laboratoire Léon Brillouin (LLB, Saclay, France), IN3 at the Institute Laue Langevin in Grenoble (France), and PUMA at the research neutron source Heinz Maier-Leibnitz in Garching (Germany). Two single crystals with different compositions have been grown using the Czochralski method. The chemical composition has been measured by Elastic Recoil Detection: $Ni_{51}Mn_{18}Al_{31}$ and $Ni_{53}Mn_{22}Al_{25}$, yielding e/a ratios of 7.29 and 7.59, respectively. To retain the B2 phase at low temperature, the samples have been annealed in fused-quartz tubes under argon atmosphere at 1273 K during three days and subsequently water quenched. The crystals have been oriented to have their (001) plane coincide with the scattering plane. However, a repositioning of the $Ni_{51}Mn_{18}Al_{31}$ sample within the (110) scattering plane was necessary to measure the phonon dispersions along the $[\xi\xi\xi]$ direction. The high-temperature measurements have been performed with the samples mounted on a niobium holder in a vacuum furnace. Measurements below room temperature have been performed with the samples mounted in an aluminum container under helium atmosphere attached to the cold head of a closed-cycle cryostat. The temperature value was stable within ± 1 K during the measurements. The crystals were aligned by tilting the furnace/cryostat with a two-axis goniometer. Phonon measurements have been mainly performed in the k_f-constant mode using a pyrolytic graphite PG(002) analyzer. Scans have been performed either in the $\hbar\omega$-constant mode or $\mathbf{q}$-constant mode depending on the position of the resolution ellipsoid on the dispersion curve at the measured $(\mathbf{q},\omega)$ point.

A. Phonon dispersion curves

Phonon frequencies in $Ni_{51}Mn_{18}Al_{31}$ have been measured along the high-symmetry directions: $[\xi 00]$, $[\xi\xi 0]$, and $[\xi\xi\xi]$ in the B2 phase at 298 K. The dispersion curves have been fitted to the measured phonon frequencies $[\omega(\mathbf{q})]$ using the harmonic approximation within the Born–von Kármán (BVK) model.[21] This force-constant model assumes that the potential energy of the crystal is a sum of spherical two-body potentials taken over all the pairs of atoms. The interaction between any two atoms at any distance from each other is

TABLE I. Longitudinal (f_l) and transverse (f_t) force constants (in N/m) determined by fitting the BVK model to measured phonon frequencies in B2-$Ni_{51}Mn_{18}Al_{31}$ at 298 K. The notation A-B^n indicates nth neighbor A-B pairs.

Pair	f_l	f_t
Ni-Mn/Al[1]	31.0	0.7
Ni-Ni[2]	1.4	1.3
Al-Al[2]	11.2	−1.4
Ni-Ni[3]	5.3	−1.7
Al-Al[3]	0.5	0.00
Ni-Al/Mn[4]	−0.3	−0.2
Ni-Ni[5]	0.3	0.0
Al-Al[5]	2.5	0.0

reduced to two force constants. One for the longitudinal elongation and one for the transverse elongation. The appropriate number of neighbor shells is found by trial: the maximum shell radius of considered neighbors is increased until the fit quality converges. In order do describe the phonon dispersion of B2-$Ni_{51}Mn_{18}Al_{31}$ adequately, five nearest-neighbor shells have been taken into account. The force constants deduced from the fit are listed in Table I.

The phonon-dispersion curves of B2-$Ni_{51}Mn_{18}Al_{31}$ are depicted in Fig. 4. As the unit cell of the B2 structure contains two atoms, there are six phonon branches, three acoustic and three optical. The acoustic and optical branches are separated by a gap between 5.6 and 6.5 THz. The transverse branches are doubly degenerated along the $[\xi 00]$ and $[\xi\xi\xi]$ directions, a common point to cubic systems. The most important features of the phonon dispersions are the kink observed in the $TA_2[\xi\xi 0]$ branch in the ξ range 0.1–0.25 rlu and the small dip in the $LA[\xi\xi\xi]$.

Using the atomic force constants obtained from the BVK fits, the total and the partial phonon density of states (DOS) $Z(\omega)$ in $Ni_{51}Mn_{18}Al_{31}$ are obtained from the dispersion relations $\omega(\mathbf{q})$ by integration over the first Brillouin zone using the method first proposed by Gilat and Raubenheimer.[22] The phonon DOS plot (Fig. 5) reflects the typical features of the phonon-dispersion curves with a gap between 5.6 and 6.5 THz showing a clear separation between the acoustic and optical modes as well as a cutoff frequency of 8.4 THz. The low-frequency part of the density of states consists mostly of the contribution of the heavier atoms (Ni, dashed curve), while the contribution of the lighter atoms (Al/Mn, dotted curve) dominates at the uppermost frequency range, above 6.5 THz. This sustains a normal behavior of the different atomic species contribution to the total DOS contrary to the predictions of first-principles calculations in Ni-based Heusler unstable systems.[23] From the phonon DOS, we have calculated the Debye temperature, the average vibration entropy per atom, and the specific heat per atom within the harmonic approximation.[24,25] These values are summarized together in Table II.

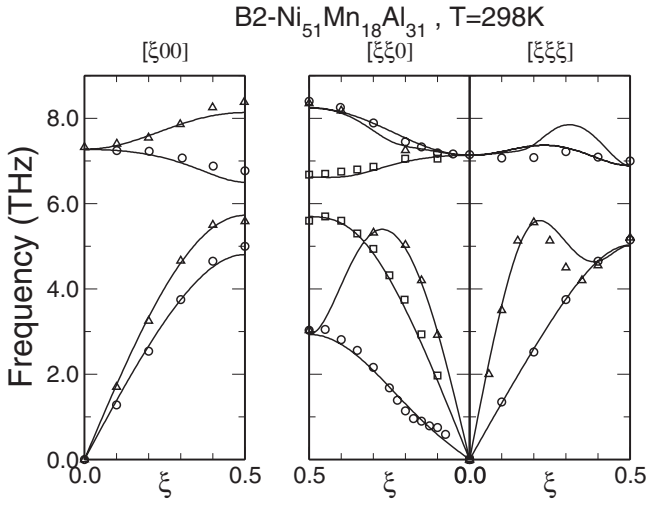

FIG. 4. Phonon dispersions of B2-$Ni_{51}Mn_{18}Al_{31}$ along $[\xi 00]$, $[\xi\xi 0]$, and $[\xi\xi\xi]$ directions at 298 K. The solid lines indicate dispersion curves determined by fitting the force constants from the Born–von Kármán model to the experimental data.

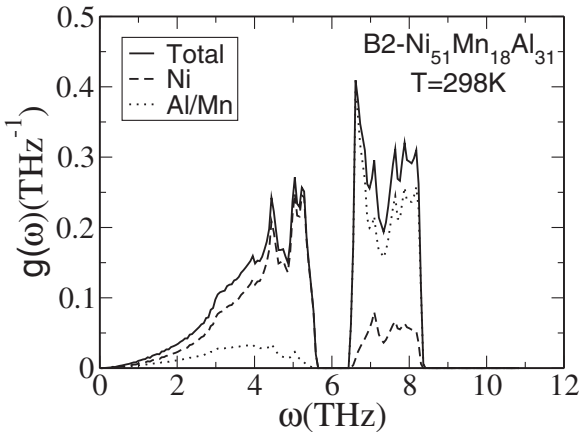

FIG. 5. Total and partial phonon densities of states in $Ni_{51}Mn_{18}Al_{31}$ calculated from the Born–von Kármán force constants. Note the normal contribution of the different atomic species. Namely, the low-frequency part of the density of states consists mostly of the contribution of the heavier atoms (Ni, dashed curve), while the contribution of the lighter atoms (Al/Mn, dotted curve) appears dominantly at the uppermost frequency range above 6.5 THz.

B. $TA_2[\xi\xi 0]$ phonon softening

Acoustic phonons measured in $Ni_{51}Mn_{18}Al_{31}$ and in $Ni_{53}Mn_{22}Al_{25}$ at different temperatures are depicted in Fig. 6. Overall, the phonon frequencies of acoustic branches are comparable to those reported in other Ni_2MnAl alloys with a

TABLE II. Thermodynamic properties calculated from the phonon density of states of $Ni_{51}Mn_{18}Al_{31}$ at room temperature. S_V refers to the vibrational entropy per atom, θ_D to Debye temperature, C_V to specific heat per atom, and u^2 to the mean-square displacements.

$C_V(k_B)$	θ_D (K)	$S_v(k_B)$	$u^2_{Mn/Al}(Å^2)$	$u^2_{Ni}(Å^2)$
2.78	372	3.55	0.0024	0.0070

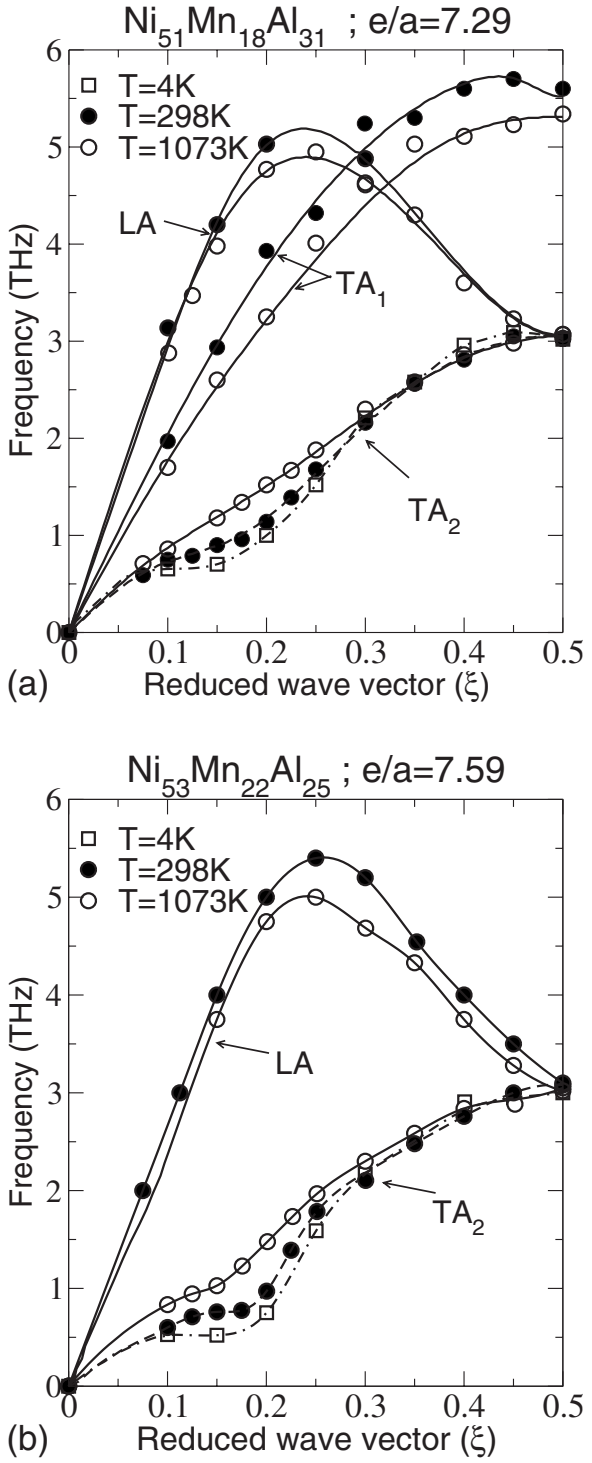

FIG. 6. Temperature dependence of the acoustic phonon branches along $[\xi\xi 0]$ in B2-$Ni_{51}Mn_{18}Al_{31}$ (top, $e/a=7.29$) and B2-$Ni_{53}Mn_{22}Al_{25}$ (bottom, $e/a=7.59$). Note the anomalous softening of the $TA_2[\xi\xi 0]$ phonons in the range 0.1–0.25 rlu of ξ. The lines are guide to the eyes.

composition close to those of the crystals investigated here.[26] The phonon frequencies of the $TA_2[\xi\xi 0]$ branch measured in Ni_2MnAl show higher values compared to those of Ni_2MnGa.[9,10] This is consistent with the fact that the studied crystals do not transform martensitically within the studied

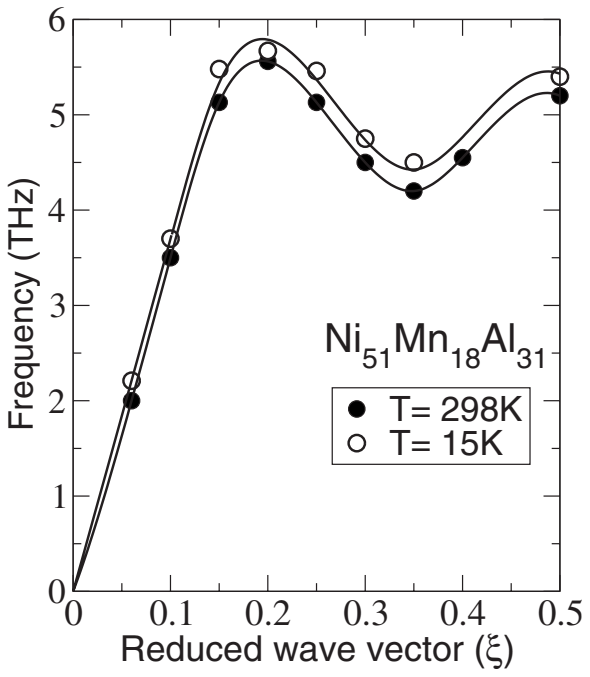

FIG. 7. Temperature dependence of the $LA[\xi\xi\xi]$ measured in B2-$Ni_{51}Mn_{18}Al_{31}$ at 298 and 15 K. The solid lines are guide to the eyes. Note the normal softening with increasing temperature.

temperature range. A general trend found from the phonon spectra is an overall lowering of the frequencies with increasing temperature presumably due to increasing anharmonic effects. A typical normal temperature dependence of the phonon frequencies is shown in Fig. 7 where a small decrease in the $LA[\xi\xi\xi]$ phonon frequencies with increasing temperature is seen. Contrary to the overall behavior, the $TA_2[\xi\xi 0]$ phonon branch with the polarization $\{1\bar{1}0\}$ shows an anomalous softening with decreasing temperature, associated with a wiggle in the ξ range 0.1–0.25 rlu. This behavior is a signature of low-restoring forces against the sliding of the (110) atomic planes in the $[1\bar{1}0]$ direction. Such displacements associated with atomic shuffles in the (110) planes could constitute basal planes of the close-packed structure if the sample transformed into the martensitic phase at low temperature. In both samples, the wiggle deepens with decreasing temperature but does not result in any clear minimum down to the lowest measured temperature. The measured data are fitted with a damped harmonic oscillator yielding a damping Γ (full width at half maximum) which does not show any anomalous behavior in particular when compared to the damping observed in the bcc phase of the elementary systems Ti, Zr, and Hf.[3,4] The phonons are well defined over the whole ξ range. Figure 8 shows the temperature dependence of Γ deduced from the fit of the $TA_2[\xi\xi 0]$ phonons measured in $Ni_{51}Mn_{18}Al_{31}$. An increase in the linewidth of the phonons is observed near the zone boundary presumably due to the superposition to the phonon signal of the incoherent scattering of Ni.

The measured phonon behavior agrees quite well with the prediction of recent *ab initio* calculations. Based on density-functional theory, Bügsen *et al.*[27] calculated the phonon-

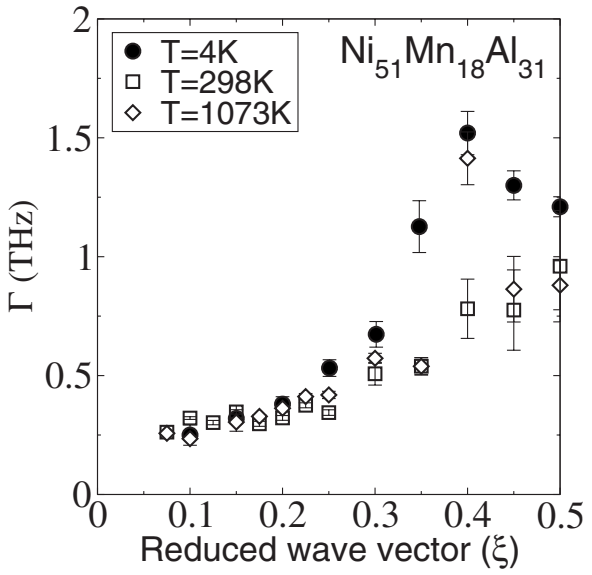

FIG. 8. Temperature dependence of the damping Γ of the $TA_2[\xi\xi 0]$ phonon branch as measured in $Ni_{51}Mn_{18}Al_{31}$.

dispersion curves in Heusler $L2_1$-Ni_2MnAl along $[\xi\xi 0]$. They predicted complete softening of the $TA_2[\xi\xi 0]$ branch in ξ range 0.25–0.4 rlu. Despite the difference in the state of order, the extension of the phonon anomaly in **q** space compares quite good considering that the lattice parameter of the $L2_1$ phase is twice higher than that of the B2 phase. The character of the phonon anomaly measured in Ni_2MnAl resembles that one observed in NiAl.[8] In both cases, the wiggle observed in the $TA_2[\xi\xi 0]$ branch does not develop to a clear minimum upon cooling. It has been argued for Ni-Al (Ref. 8) that the phonon dip never gets deep enough and the strain energy associated with the corresponding wave vector is not sufficiently large to induce a modulation in the low-temperature martensite. Whether this argument holds also for Ni_2MnAl cannot be concluded here because both samples $Ni_{51}Mn_{18}Al_{31}$ and $Ni_{53}Mn_{25}Al_{22}$ do not undergo a martensitic transformation down to the lowest measured temperatures.

A careful comparison of the $TA_2[\xi\xi 0]$ phonon frequencies measured in $Ni_{51}Mn_{18}Al_{31}$ and in $Ni_{53}Mn_{22}Al_{25}$ reveals subtle differences. On the first hand, the dispersion of the $TA_2[\xi\xi 0]$ branch measured at 1073 K in $Ni_{53}Mn_{22}Al_{25}$ shows a tiny wiggle around $\xi=0.15$ rlu whereas the same branch recovers fully the sinuslike behavior in $Ni_{51}Mn_{18}Al_{31}$ at the same temperature. On the second hand, the absolute values of the phonons frequencies are smaller in $Ni_{53}Mn_{22}Al_{25}$ compared to $Ni_{51}Mn_{18}Al_{31}$. This is clearly seen if the phonon frequencies are normalized to the zone-boundary frequency to get rid of the effect of the mass. The normalized frequencies are up to 20% smaller in $Ni_{53}Mn_{22}Al_{25}$ within the ξ range where the phonon anomaly is seen (Fig. 9). The present phonon measurements give a simple picture on the atomic scale of the increasing lattice instability with increasing e/a as observed in the DSC measurements; the restoring forces against the shearing of the (110) atomic planes along $\{1\bar{1}0\}$ are weaker at higher e/a. This tendency has been predicted from *ab initio* calculations in Ni_2MnGa.[28]

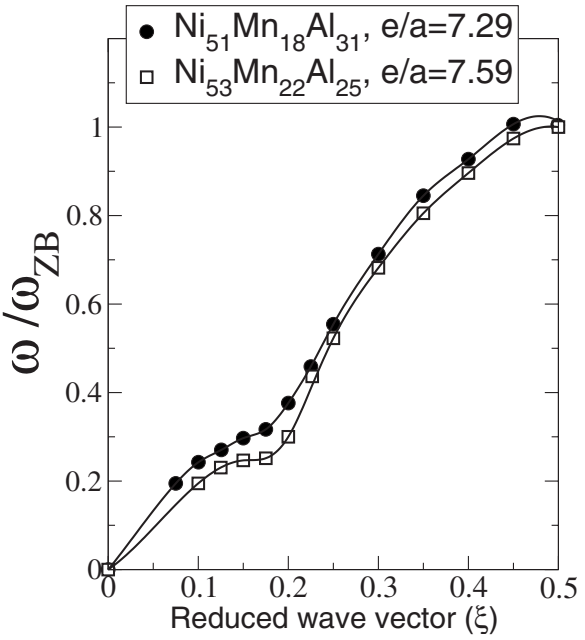

FIG. 9. Phonon frequencies of the $TA_2[\xi\xi 0]$ normalized to the zone-boundary phonon frequency ω_{ZB} measured at room temperature in $Ni_{51}Mn_{18}Al_{31}$ ($e/a=7.29$) and in $Ni_{53}Mn_{22}Al_{25}$ ($e/a=7.59$). The solid lines are guide to the eyes.

In order to investigate the effect of the atomic ordering on the lattice dynamics, a $Ni_{51}Mn_{18}Al_{31}$ single crystal has been annealed in a quartz tube under argon atmosphere at 673 K, below the $B2 \rightarrow L2_1$ ordering temperature (700 K) reported in the literature,[13] during 45 days. Despite of the very-long annealing time, neutron diffraction performed on the single crystal revealed only a weak $L2_1$ ordering. The $L2_1$ order parameter was not exceeding 10%. Whether the missing single $L2_1$ phase is due to a too short annealing time or a metastable equilibrium between the B2 and the $L2_1$ phases is reached is unclear. The annealed $Ni_{51}Mn_{18}Al_{31}$ has been aligned to have its (001) plane coincide with the scattering plane to access the $TA_2[\xi\xi 0]$ phonon branch which has been measured at different temperatures. Figure 10 displays the temperature dependence of the $TA_2[\xi\xi 0]$ phonon branch. Again a wiggle is observed in the ξ range 0.1–0.25 rlu. The wiggle deepens with decreasing temperatures but does not result in any clear minimum down to 16 K. The comparison of the $TA_2[\xi\xi 0]$ phonon softening in the as-quenched and in the annealed crystals reveals clear differences. This is seen in Fig. 11 where the frequency squared of the $TA_2[\xi\xi 0]$ phonon modes for $\xi=0.15$ and $\xi=0.2$ in the two crystals are reported as function of temperature. In good agreement with the Landau theory for phase transitions, the data are well fitted with linear regressions.[29] However, the degree of softening, given by the slope, is, below 673 K, smaller in the annealed sample. Because of the weak $L2_1$ order, the difference in the degree of softening is most likely due to the formation of precipitates during the very-long annealing time. Optical micrographs and DSC measurements performed on polycrystalline samples annealed in the same conditions support this idea. The formation of precipitates leads to changes in the chemical composition of the matrix which directly affect the

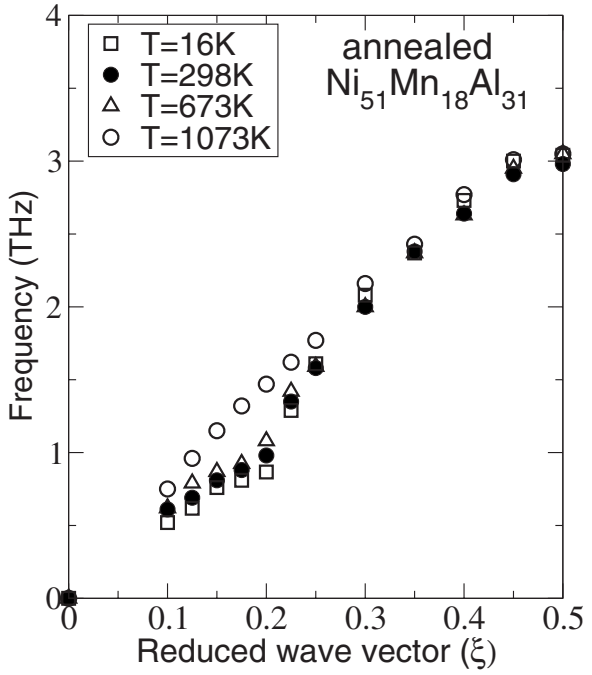

FIG. 10. Temperature dependence of the $TA_2[\xi\xi 0]$ phonon frequencies measured in a $Ni_{51}Mn_{18}Al_{31}$ crystal annealed at 673 K during 45 days.

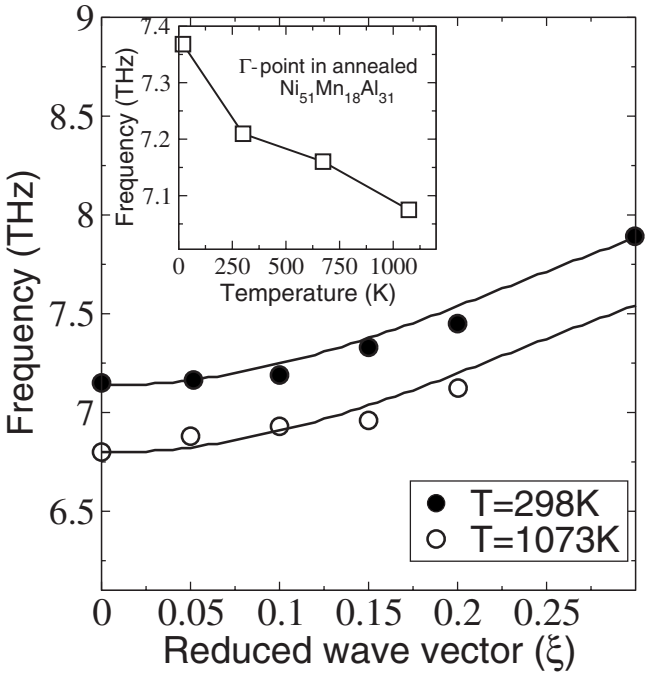

FIG. 12. Temperature dependence of the $TO_2[\xi\xi 0]$ phonon modes in B2-$Ni_{51}Mn_{18}Al_{31}$ measured close to the Γ point. The inset shows the frequency of the Γ point measured in the annealed $Ni_{51}Mn_{18}Al_{31}$ crystal. Note the normal softening with increasing temperature in both crystals.

phonon frequencies of the $TA_2[\xi\xi 0]$ branch as seen in Figs. 6 and 9.

In good agreement with previous phonon measurements on a $Ni_{54}Mn_{23}Al_{23}$ single crystal,[26] the degree of softening is not enhanced when the system orders in the antiferromagnetic state below room temperature. However, ultrasonic measurements under applied magnetic field revealed that the value of the elastic constants in Ni_2MnAl depends on the magnetic order,[30] giving an evidence of the coupling of the magnetism to the lattice. It has been argued for Ni_2MnGa that the degree of softening is strongly enhanced when the system orders in the ferromagnetic state leading to an inflexion point in the curve of ω^2 versus temperature. The coincidence of the Curie temperature with the inflexion point suggests that the magnetization of the sample influences the phonon energy through the so-called magnetoelastic coupling.[10] This coupling has been described by adding a term, proportional to the square of magnetization, to the free energy of the system. The weak magnetization of antiferromagntic Ni_2MnAl compared to the ferromagnetic Ni_2MnGa can explain the different impacts of the magnetic ordering on the phonon softening.

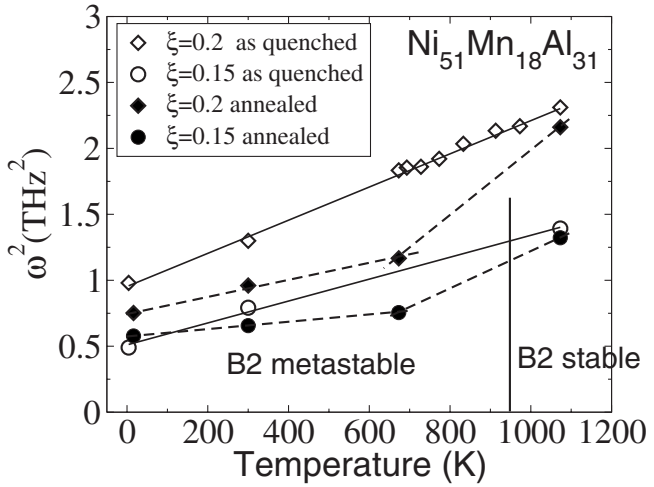

FIG. 11. Temperature dependence of the frequency squared of the $TA_2[\xi\xi 0]$ phonon modes for $\xi=0.15$ and $\xi=0.20$ as measured in the as-quenched (open symbols) and in the annealed (filled symbols) $Ni_{51}Mn_{18}Al_{31}$ crystal.

C. $TO_2[\xi\xi 0]$ phonons

According to recent *ab initio* calculations performed in Ni-based $L2_1$ Heusler alloys, the phonon anomaly is not restricted to acoustic modes only. It was argued that the $TA_2[\xi\xi 0]$ phonon mode is unstable because it is pushed down by from the symmetry corresponding optical mode.[15] Besides, Ni has been found to vibrate at anomalously low frequencies in Ni_2MnGa leading to an inversion in the contribution of the different atomic species to the total DOS. This acoustic-optical interaction might be of more general interest and has to be investigated in more detail including other alloy systems. Motivated by these statements, the temperature dependence of the acoustic phonon frequencies has been extended to the optical modes of the same polarization as the $TA_2[\xi\xi 0]$, namely the $TO_2[\xi\xi 0]$. Figure 12 shows the $TO_2[\xi\xi 0]$ phonon frequencies measured close to the Γ point at room temperature and at 1073 K in $Ni_{51}Al_{31}Mn_{18}$. A normal softening with increasing temperature is seen. The inves-

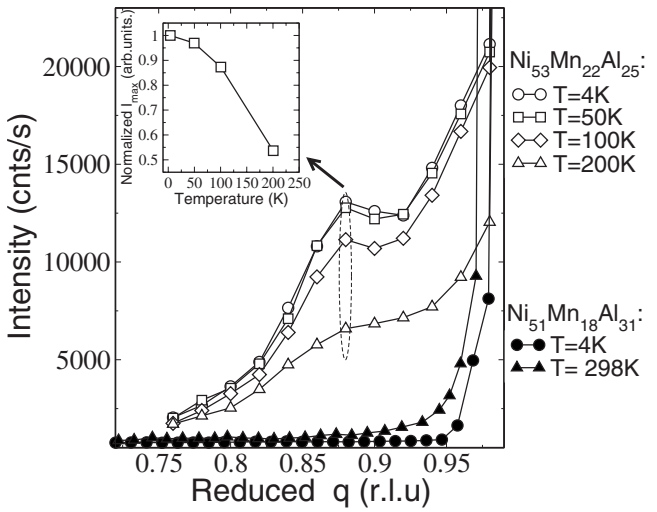

FIG. 13. Temperature dependence of the elastic scattering in $Ni_{51}Mn_{18}Al_{31}$ and $Ni_{53}Mn_{22}Al_{25}$ along $[1\bar{1}0]$ starting from the (110) reflection. The inset shows the normalized maximum intensity of the elastic signal measured at q=0.875 rlu (ξ=0.125 rlu) in $Ni_{53}Mn_{22}Al_{25}$.

tigation of optical modes has been extended to the long-time annealed $Ni_{51}Al_{31}Mn_{18}$ sample by measuring the temperature dependence of the phonon frequency at the Γ point (inset of Fig. 12). Again a normal temperature dependence is seen. Contrary to the predictions of the first-principles calculations in Ni-based $L2_1$ Heusler alloys, the $TO_2[\xi\xi 0]$ in Ni_2MnAl seems not to play an important role on the lattice instability. Indeed, the $TA_2[\xi\xi 0]$ and the $TO_2[\xi\xi 0]$ have opposite temperature behaviors.

IV. ELASTIC SCATTERING

Elastic neutron scattering has been performed on $Ni_{51}Mn_{18}Al_{31}$ and $Ni_{53}Mn_{22}Al_{25}$ crystals. The (001) scattering plane has been scanned at different temperatures with transverse scans along $[1\bar{1}0]$ starting from the fundamental reflection (110) along the $[\bar{1}10]$. Results in $Ni_{53}Mn_{22}Al_{25}$ are shown in Fig. 13. A diffuse elastic scattering is observed in $Ni_{53}Mn_{22}Al_{25}$. A diffuse intensity develops in the range 0.05–0.2 of ξ which corresponds to the position of the wiggle observed in the $TA_2[\xi\xi 0]$ phonon branch. The signal intensity increases with decreasing temperatures but does not develop in a sharp elastic peak down to 4 K. The inset of Fig. 13 shows the temperature dependence of the maximum intensity of the observed satellite normalized to the value at T=4 K. In addition to the satellite peak, there is an intense scattering that diverges as $\xi \rightarrow 0$. This scattering is a ridge or streak emanating from the (110) Brillouin-zone center. The striking feature is that no diffuse elastic signal has been observed in $Ni_{51}Mn_{18}Al_{31}$ from 298 down to 4 K (full symbols in Fig. 13).

Elastic neutron scattering has been recently performed in $Ni_{54}Mn_{23}Al_{23}$ single crystal.[26] The measurements revealed two distinct satellite peaks, one associated with the anomalous dip in the $TA_2[\xi\xi 0]$ phonon branch and one attributed to an eventual splitting of the Bragg peak owing to a tetragonal distortion as reported in Ni_2MnGa from x rays[31] and neutron scattering.[32] The difference in the behavior of the different samples suggests that such satellite peaks are sample dependent and can be related to the inhomogeneity of the sample under study. This is consistent with the fact that the martensitic transition temperature in these alloy systems is extremely sensitive on composition, and therefore the existence of small amount of martensite growing as temperature decreases cannot be completely disregarded. Besides, a comparison of the electron per atom ratio and the phonon frequencies of the $TA_2[\xi\xi 0]$ phonon branch of the two samples might suggest that the $Ni_{53}Al_{22}Mn_{25}$ was measured in its pretransitional state.

V. CONCLUSION

The interplay of structural instability and lattice dynamics in Ni_2MnAl has been investigated by calorimetry and inelastic neutron scattering. The tendency of Ni_2MnAl to undergo a martensitic transition shows up in the anomalous phonon softening of the specific $TA_2[\xi\xi 0]$ in the ξ range 0.10–0.25 rlu. which corresponds to the pattern of atomic shuffles of the modulated 2M, 10M, 12M, and 14M martensites observed in Ni_2MnAl. The phonon spectra provide a simple picture on the atomic scale of the increasing lattice instability with the electron concentration. Namely, the effective restoring forces against atomic displacements within the (110) planes in the $\{1\bar{1}0\}$ direction decrease with increasing e/a. The phonon anomaly is not enhanced when the systems orders in the antiferromagnetic state. Contrary to the predictions of the *ab initio* calculations in $L2_1$ Heusler alloys, no anomalous phonon softening of the optical phonons with the same polarization as $TA_2[\xi\xi 0]$ is observed in B2-Ni_2MnAl. Whether the discrepancy between the measurements in the B2 phase and the calculations in the $L2_1$ is due to the difference in the atomic ordering itself or to the different induced magnetic orders cannot be concluded here.

[1] A. D. Bruce and R. A. Cowley, *Structural Phase Transitions* (Taylor & Francis, London, 1981).

[2] T. Saburi, in *Shape Memory Materials*, edited by K. Otsuka and C. M. Wayman (Cambridge University Press, Cambridge, England, 1998).

[3] W. Petry, A. Heiming, J. Trampenau, M. Alba, C. Herzig, H. R. Schober, and G. Vogl, Phys. Rev. B **43**, 10933 (1991).

[4] J. Trampenau, A. Heiming, W. Petry, M. Alba, C. Herzig, W. Miekeley, and H. R. Schober, Phys. Rev. B **43**, 10963 (1991).

[5] Ll. Mañosa, J. Zarestky, T. A. Lograsso, D. W. Delaney, and C.

Stassis, Phys. Rev. B **48**, 15708 (1993).
[6] Ll. Mañosa, J. Zarestky, M. Bullock, and C. Stassis, Phys. Rev. B **59**, 9239 (1999).
[7] K. Nicolaus, Ph.D. thesis, Technical University Munich, 2000.
[8] S. M. Shapiro, B. X. Yang, Y. Noda, L. E. Tanner, and D. Schryvers, Phys. Rev. B **44**, 9301 (1991).
[9] C. Kappler, M. B. Walker, and J. Luettmer-Strathmann, Phys. Rev. B **51**, 11319 (1995).
[10] Ll. Mañosa, A. Planes, J. Zarestky, T. Lograsso, D. L. Schlagel, and C. Stassis, Phys. Rev. B **64**, 024305 (2001).
[11] A. Sozinov, A. A. Likhachev, N. Lanska, and K. Ullako, Appl. Phys. Lett. **80**, 1746 (2002).
[12] S. Morito and K. Otsuka, Mater. Sci. Eng., A **208**, 47 (1996).
[13] R. Kainuma, F. Gejima, Y. Sutou, I. Ohnuma, and K. Ishida, Mater. Trans., JIM **41**, 943 (2000).
[14] M. Acet, E. Duman, E. F. Wassermann, Ll. Mañosa, and A. Planes, J. Appl. Phys. **92**, 3867 (2002).
[15] A. T. Zayak, P. Entel, K. M. Rabe, W. A. Adeagbo, and M. Acet, Phys. Rev. B **72**, 054113 (2005).
[16] N. Lanska, O. Söderberg, A. Sozinov, Y. Ge, K. Ullako, and V. K. Lindros, J. Appl. Phys. **95**, 8074 (2004).
[17] T. Krenke, M. Acet, E. F. Wassermann, X. Moya, Ll. Mañosa, and A. Planes, Phys. Rev. B **73**, 174413 (2006).
[18] T. Krenke, M. Acet, E. F. Wassermann, X. Moya, L. Mañosa, and A. Planes, Phys. Rev. B **72**, 014412 (2005).
[19] M. Khan, I. Dubenko, S. Stadler, and N. Ali, J. Phys.: Condens. Matter **16**, 5259 (2004).
[20] R. Kainuma, M. Ise, K. Ishikawa, I. Ohnuma, and K. Ishida, J. Alloys Compd. **269**, 173 (1998).
[21] G. W. Lehman, T. Wolfram, and R. E. De Wames, Phys. Rev. **128**, 1593 (1962).
[22] G. Gilat and L. J. Raubenheimer, Phys. Rev. **144**, 390 (1966).
[23] P. Entel, V. D. Buchelnikov, V. Khovailo, A. T. Zayak, W. A. Adeagbo, M. E. Gruner, H. C. Herper, and E. F. Wassermann, J. Phys. D **39**, 865 (2006).
[24] M. A. Krivoglaz, *Theory of X-Ray and Thermal Neutron Scattering by Real Crystals* (Plenum, New York, 1969).
[25] C. Kittel, *Introduction to Solid State Physics* (Wiley, New York, 1976).
[26] X. Moya, L. Mañosa, A. Planes, T. Krenke, M. Acet, V. O. Garlea, T. A. Lograsso, D. L. Schlagel, and J. L. Zarestky, Phys. Rev. B **73**, 064303 (2006).
[27] T. Büsgen, J. Feydt, R. Hassdorf, S. Thienhaus, M. Moske, M. Boese, A. Zayak, and P. Entel, Phys. Rev. B **70**, 014111 (2004).
[28] A. T. Zayak, W. A. Adeagbo, P. Entel, and K. M. Rabe, Appl. Phys. Lett. **88**, 111903 (2006).
[29] J. A. Krumhansl, Solid State Commun. **84**, 251 (1992).
[30] X. Moya, Ll. Mañosa, A. Planes, T. Krenke, M. Acet, M. Morin, J. L. Zarestky, and T. A. Lograsso, Phys. Rev. B **74**, 024109 (2006).
[31] G. Fritsch, V. V. Kokorin, and A. Kempf, J. Phys.: Condens. Matter **6**, L107 (1994).
[32] U. Stuhr, P. Vorderwisch, V. V. Kokorin, and P.-A. Lindgard, Phys. Rev. B **56**, 14360 (1997).